

Unstructured flux-limiter convective schemes for simulation of transport phenomena in two-phase flows ^{*}

Néstor Balcázar-Arciniega¹[0000-0003-0776-2086], Joaquim Rigola¹[0000-0002-6685-3677], and Assensi Oliva¹[0000-0002-2805-4794]

¹ Heat and Mass Transfer Technological Center (CTTC), Universitat Politècnica de Catalunya-BarcelonaTech (UPC). Colom 11, 08222, Terrassa (Barcelona), Spain
nestor.balcazar@upc.edu, nestorbalcazar@yahoo.es

Abstract. Unstructured flux-limiters convective schemes designed in the framework of the unstructured conservative level-set (UCLS) method, are assessed for transport phenomena in two-phase flows. Transport equations are discretized by the finite volume method on 3D collocated unstructured meshes. The central difference scheme discretizes the diffusive term. Gradients are evaluated by the weighted least-squares method. The fractional-step projection method solves the pressure-velocity coupling in momentum equations. Numerical findings about the effect of flux limiters on the control of numerical diffusion and improvement of numerical stability in DNS of two-phase flows are reported.

Keywords: Unstructured Flux-Limiters · Finite-Volume Method · Unstructured Meshes · Unstructured Conservative Level-Set Method · Mass transfer · Direct Numerical Simulation · High-Performance Computing

1 Introduction

Transport phenomena in two-phase flows are prevalent in natural and industrial processes, playing crucial roles in various engineering devices, from steam generators to cooling towers in thermal power plants and the so-called unit operations of chemical engineering. Bubbles and droplets are essential in separation processes such as distillation or promoting chemical reactions in industrial devices. Beyond its scientific significance, a profound comprehension of the intricate interplay between fluid mechanics and transport phenomena in multiphase flows is indispensable for designing and optimising engineering systems involving multiple phases.

Experimental exploration of two-phase flows, particularly bubbly flows, is constrained by optical access. Analytical methods involve significant simplifications of physical models. In contrast, computational methods, such as Direct Numerical Simulation (DNS) of two-phase flows [39,49], have been empowered with the advent of

^{*} The principal author, N. Balcázar-Arciniega, as Serra-Hunter Lecturer (UPC-LE8027), acknowledges the financial support provided by the Catalan Government through this program. Simulations were conducted using computing resources allocated by the Spanish Supercomputing Network (RES) under the grants IM-2023-2-0009, IM-2023-1-0003 on the supercomputer MareNostrum IV in Barcelona, Spain. The financial support of the MINECO, Spain (grant PID2020-115837RB-100), is acknowledged.

supercomputing capabilities. Several approaches, including front-tracking (FT) [50,48], level-set (LS) [37,44,27], conservative level-set (CLS) [36,7,12], Volume of Fluid (VoF) [29], and coupled VoF-LS [43,42,8], have been proposed for DNS of two-phase flow. In further developments these methods have been applied to mass transfer and heat transfer in single bubbles [23,17,21], bubble swarms [1,41,33,13,12,14], variable surface tension [10,14], and liquid-vapor phase change [16].

Numerical challenges for the DNS of two-phase flows include the so-called numerical diffusion [38], numerical oscillations around discontinuities, the computational cost of solving the Poisson equation in two-phase flow with high-density ratio, numerical coalescence in bubble swarms, and accurate computation of surface tension forces. These issues have been effectively tackled within the framework of the Unstructured Conservative Level-Set (UCLS) method proposed by Balcazar et al. [13,9,7,4,10,15,14,16,2]. The UCLS method employs a carefully tuned level-set function to set the interface thickness. Additionally, the least-squares method accurately computes normal vectors perpendicular to the interface, leading to a precise calculation of surface tension forces. Moreover, physical properties are smoothed across the interface using the conservative level-set function to prevent numerical oscillations. The so-called numerical coalescence of bubbles is avoided by the multiple marker approach [9,13].

This research focuses on assessing unstructured flux-limiter convection schemes proposed by Balcazar et al. [7,13] in the framework of the UCLS method. An appropriate selection of flux-limiters in DNS of interfacial transport phenomena leads to minimising the so-called numerical diffusion and preventing numerical oscillations across the fluid interface. This assessment is particularly relevant in bubbly flows with high physical properties ratios and predicting mass transfer coefficients (Sherwood number) for interfacial transport processes. It is worth mentioning that flux-limiter schemes have been designed initially for regular and Cartesian meshes [46,34,35], whereas some further efforts have been reported on unstructured meshes [22,30,7,25,52,12]. Nevertheless, the impact of unstructured flux limiters on the simulation of transport phenomena in two-phase flows, e.g., interfacial heat transfer and mass transfer, needs additional research. This work contributes to filling this gap, as well as to the development of numerical models for transport phenomena in two-phase flows.

This paper is organised as follows: The mathematical formulation and numerical methods are introduced in Section 2. Section 3 reports numerical experiments on the impact of flux-limiter schemes. Finally, conclusions and future work are outlined in Section 4.

2 Mathematical Formulation and Numerical Methods

2.1 Transport Equations

The Navier-Stokes equations for the dispersed phase (Ω_d) and continuous phase (Ω_c) are solved in the framework of the one-fluid formulation [49,39] and the multi-marker UCLS approach [12,14], as follows:

$$\frac{\partial}{\partial t}(\rho\mathbf{v}) + \nabla \cdot (\rho\mathbf{v}\mathbf{v}) = -\nabla p + \nabla \cdot \mu(\nabla\mathbf{v}) + \nabla \cdot \mu(\nabla\mathbf{v})^T + (\rho - \rho_0)\mathbf{g} + \mathbf{f}_\sigma, \quad (1)$$

$$\nabla \cdot \mathbf{v} = 0, \quad (2)$$

where \mathbf{v} is the fluid velocity, p is the pressure, ρ is the fluid density, μ is the dynamic viscosity, \mathbf{g} refers to the gravitational acceleration, \mathbf{f}_σ is the surface tension force per unit volume concentrated on the interface. Subscripts d and c refer to the dispersed and continuous phases, respectively. Density and viscosity are constant at each fluid phase, with a jump discontinuity across the interface: $\rho = \rho_c H_c + \rho_d H_d$, $\mu = \mu_c H_c + \mu_d H_d$. Here, H_c is the Heaviside step function, which is one in Ω_c and zero in Ω_d . Furthermore, $H_d = 1 - H_c$. The force $-\rho_0 \mathbf{g}$ (Eq.(1)) [12,3,4], is activated if periodic boundary conditions are applied along the y -axis (parallel to \mathbf{g}), with $\rho_0 = V_\Omega^{-1} \int_\Omega (\rho_c H_c + \rho_d H_d) dV$. Otherwise, $\rho_0 = 0$.

Interface capturing is performed by the Unstructured Conservative Level-Set (UCLS) method proposed by Balcazar et al. [12,7], in the framework of 3D unstructured meshes and the finite-volume method. On the other hand, the numerical coalescence of fluid particles is avoided by the multi-marker UCLS approach [12,2,3,10,4,14]. In this context, a regularized signed distance function [12,10,7] is used for each marker, $\phi_i = \frac{1}{2} (\tanh(\frac{d_i}{2\varepsilon}) + 1)$, where d_i is a signed distance function [37,45], and ε sets the thickness of the interface profile [7,9,4,10,12]. The UCLS advection equation is solved in conservative form, for each marker:

$$\frac{\partial \phi_i}{\partial t} + \nabla \cdot \phi_i \mathbf{v} = 0, \quad i = \{1, 2, \dots, N_m - 1, N_m\}. \quad (3)$$

Here, N_m is the number of UCLS markers, which equals the number of fluid particles. To maintain the level-set profile, the following unstructured re-initialization equation [7,12] is solved:

$$\frac{\partial \phi_i}{\partial \tau} + \nabla \cdot \phi_i (1 - \phi_i) \mathbf{n}_i^0 = \nabla \cdot \varepsilon \nabla \phi_i, \quad i = \{1, 2, \dots, N_m - 1, N_m\}, \quad (4)$$

which is computed for the pseudo-time τ up to the steady state. Here, \mathbf{n}_i^0 denotes the interface normal unit vector evaluated at $\tau = 0$. At Ω_P , $\varepsilon_P = 0.5(h_P)^\alpha$, $\alpha = [0.9, 1]$ unless otherwise stated, h_P is the characteristic local grid size [12,10,7]. Interface normal vectors (\mathbf{n}_i) and curvatures (κ_i) are calculated as follows [12,4,7]: $\mathbf{n}_i = \nabla \phi_i / \|\nabla \phi_i\|^{-1}$, $\kappa_i = -\nabla \cdot \mathbf{n}_i$.

Computation of the surface tension force (\mathbf{f}_σ , Eq.(1)) is performed in the framework of the Continuous Surface Force (CSF) model [18], as extended to the multi-marker UCLS approach [4,10,3,12,14]:

$$\mathbf{f}_\sigma = \sum_{i=1}^{N_m} (\mathbf{f}_{\sigma,i}^{(n)} + \mathbf{f}_{\sigma,i}^{(t)}). \quad (5)$$

Here, the interface tangential component $\mathbf{f}_{\sigma,i}^{(t)}$, is the so-called Marangoni force [24], defined as $\mathbf{f}_{\sigma,i}^{(t)} = \nabla_{\Gamma_i} \sigma \delta_{\Gamma_i}^s$ [12,7,3,14], σ is the surface tension coefficient. If σ is constant, as in the present research, then $\mathbf{f}_{\sigma,i}^{(t)} = \mathbf{0}$. On the other hand, the normal component of the surface tension force, perpendicular to the interface (Γ_i), is calculated as $\mathbf{f}_{\sigma,i}^{(n)} = \sigma \kappa_i \nabla \phi_i$ [7,9,12].

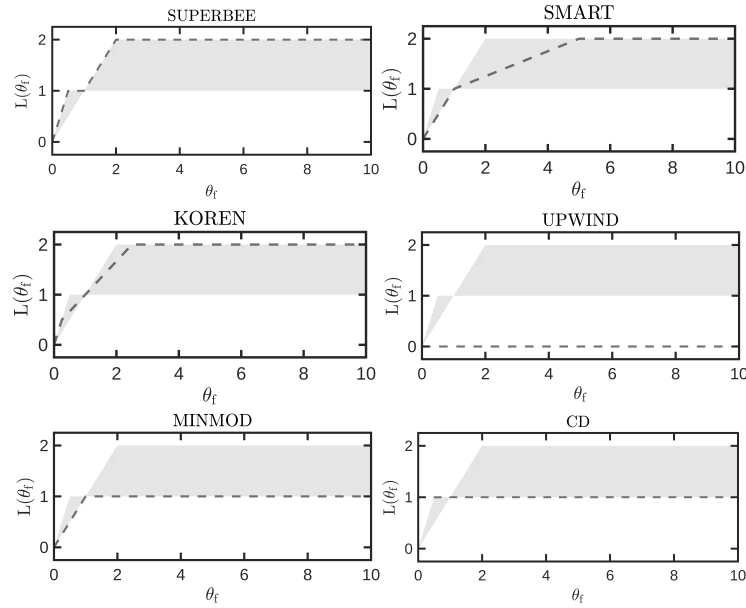


Fig. 1. Flux-limiters (dashed lines) $\psi(\theta_f)$ versus monitor variable θ_f , on the Sweby's diagram (shaded region) [46] for second-order TVD flux-limiter region.

Transport equation	Convective term	β	ψ
Eq.(1)	$\nabla \cdot \rho v_i \mathbf{v}$	ρ	v_i
Eq.(3)	$\nabla \cdot \phi \mathbf{v}$	1	ϕ
Eq.(6)	$\nabla \cdot (C \mathbf{v})$	1	C

Table 1. Convective term of transport equations. Here, v_i denotes the Cartesian components of \mathbf{v} . Correspondence of transport equations and parameters β and ψ in Eq.(7).

For external mass transfer [20], the concentration of chemical species (C) evolves according to the following transport equation:

$$\frac{\partial C}{\partial t} + \nabla \cdot (\mathbf{v}C) = \nabla \cdot (\mathcal{D}\nabla C), \quad (6)$$

which is solved in Ω_c . Here, $\mathcal{D} = \mathcal{D}_c$ is the diffusivity. The concentration of chemical species inside the bubbles is kept constant, whereas the concentration at the interface cells is calculated according to the unstructured interpolation method proposed by Balcázar-Arciniega et al. [12].

2.2 Numerical methods

The finite-volume method is used to discretize transport equations on 3D collocated unstructured meshes [12]. The convective term of transport equations are discretized

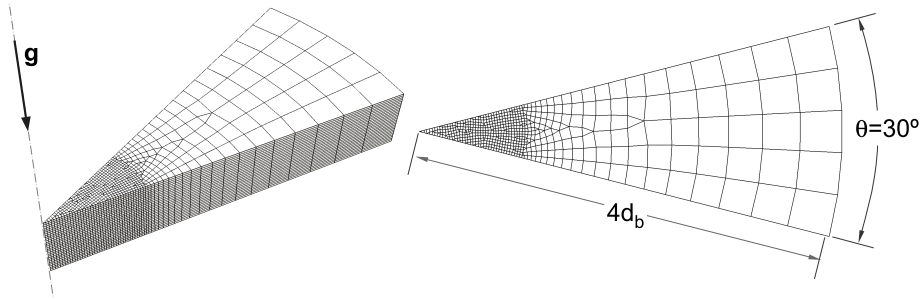


Fig. 2. Gravity-driven rising bubble. Example of mesh distribution, refined around the symmetry axis. Control volumes are a combination of hexahedrals and triangular prisms. Ω is a section of a cylindrical domain, with angle $\theta = 30^\circ$, radius $R = 4 d_b$ and height $L_y = 12 d_b$ (parallel to \mathbf{g}). Here, d_b is the spherical equivalent bubble diameter.

with unstructured flux-limiter schemes proposed by Balcazar et al. [7,12]. Indeed, at Ω_P :

$$(\nabla \cdot \beta \psi \mathbf{v})_P = V_P^{-1} \sum_f \beta_f \psi_f (\mathbf{v}_f \cdot \mathbf{A}_f), \quad (7)$$

where $\mathbf{A}_f = A_f \mathbf{e}_f$ is the area vector, subindex f denotes the cell-faces, V_P denotes the volume of Ω_P , and \mathbf{e}_f is a unit-vector pointing outside Ω_P . Moreover,

$$\psi_f = \psi_{C_p} + \frac{1}{2} L(\theta_f) (\psi_{D_p} - \psi_{C_p}), \quad (8)$$

where $\theta_f = (\psi_{C_p} - \psi_{U_p}) / (\psi_{D_p} - \psi_{C_p})$, and $L(\theta_f)$ is the flux limiter function. Furthermore, subindex D_p is the downwind point, subindex C_p is the upwind point, subindex U_p is the far-upwind point, according to the stencil proposed for the single marker and multi-marker UCLS method [12,7]. The correspondence of convective term in transport equations and Eq.(7) is outlined in Table 1. Flux-limiter functions used in this research are summarized as follows: [47,26,28,35,32]:

$$L(\theta_f) \equiv \begin{cases} \max\{0, \min\{2\theta_f, 1\}, \min\{2, \theta_f\}\} & \text{SUPERBEE,} \\ \max\{0, \min\{2\theta_f, (2/3)\theta_f + (1/3), 2\}\} & \text{KOREN,} \\ \max\{0, \min\{4\theta_f, 0.75 + 0.25\theta_f, 2\}\} & \text{SMART,} \\ (\theta_f + |\theta_f|) / (1 + |\theta_f|) & \text{VANLEER,} \\ \min\text{mod}\{1, \theta_f\} & \text{MINMOD,} \\ 0 & \text{UPWIND,} \\ 1 & \text{CD.} \end{cases} \quad (9)$$

Figure 1 summarizes the so-called Sweby's diagram for second-order Total Variation Diminishing (TVD) flux-limiters [47] and some of the functions outlined in Eq.(9). First-order accurate schemes, e.g., UPWIND, suffer from numerical diffusion, whereas

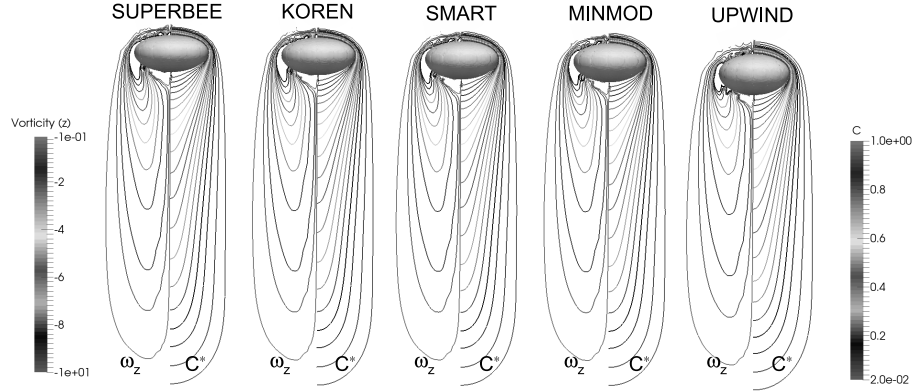


Fig. 3. Gravity-driven rising bubble. Effect of flux-limiter convective schemes on the vorticity $\omega_z = \mathbf{e}_z \cdot (\nabla \times \mathbf{v})$, and normalized concentration $C^* = C_c/C_{\Gamma,c}$ fields, at $t^* = 5$. Here, $C_{\Gamma,c}$ is the concentration of chemical species at the interface. $Eo = 3.125$, $Mo = 10^{-6}$, $Sc = 1$, $\eta_\rho = \eta_\mu = 100$.

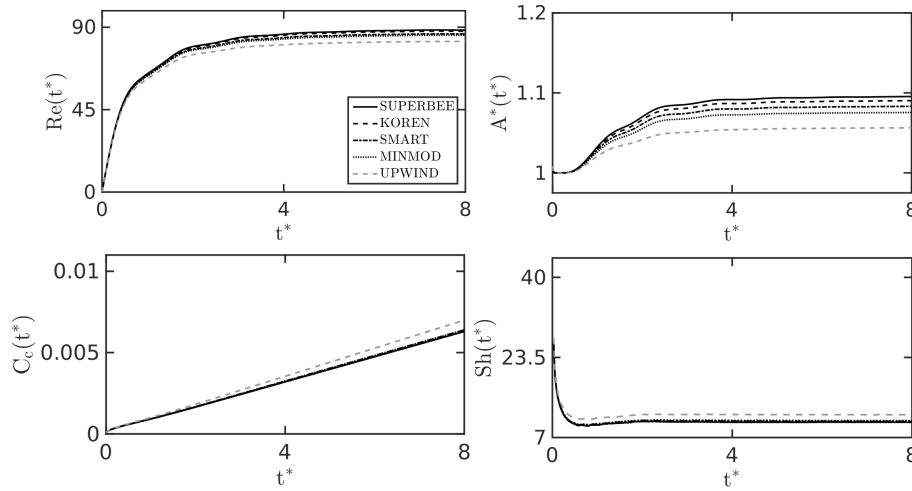


Fig. 4. Gravity-driven rising bubble. Effect of flux-limiter convective schemes on $\{Re(t^*), C_c(t^*), A^*(t^*), Sh(t^*)\}$. $Eo = 3.125$, $Mo = 10^{-6}$, $Sc = 1$, $\eta_\rho = \eta_\mu = 100$.

high-resolution schemes (SUPERBEE, KOREN, SMART, VANLEER, MINMOD) tend to minimize this numerical artefact.

Concerning the diffusive term of transport equations, a central-difference scheme [13] is used. Gradients are evaluated by the weighted least-squares method [12,7], whereas values at the cell-faces are linearly interpolated. The pressure-velocity cou-

pling is solved with the fractional-step projection method [19,39,49]:

$$\frac{\rho_P \mathbf{v}_P^* - \rho_P^0 \mathbf{v}_P^0}{\Delta t} = \mathbf{C}_{\mathbf{v},P}^0 + \mathbf{D}_{\mathbf{v},P}^0 + (\rho_P - \rho_0) \mathbf{g} + \mathbf{f}_{\sigma,P}, \quad (10)$$

$$\left(\nabla \cdot \left(\frac{\Delta t}{\rho} \nabla p \right) \right)_P = (\nabla \cdot \mathbf{v}^*)_P, \quad \mathbf{e}_{\partial\Omega} \cdot \nabla p|_{\partial\Omega} = 0. \quad (11)$$

$$\frac{\rho_P \mathbf{v}_P - \rho_P \mathbf{v}_P^*}{\Delta t} = -(\nabla p)_P. \quad (12)$$

Here, the superscript 0 refers to the previous time-step, $\mathbf{C}_{\mathbf{v}} = -\nabla \cdot (\rho \mathbf{v} \mathbf{v})$, and $\mathbf{D}_{\mathbf{v}} = \nabla \cdot \mu \nabla \mathbf{v} + \nabla \cdot \mu (\nabla \mathbf{v})^T$. The predictor velocity is \mathbf{v}_P^* , and the corrected velocity is represented by \mathbf{v}_P . A linear system arises from the finite volume approximation of Eq. (11), and it is solved using a preconditioned conjugate gradient method with a Jacobi pre-conditioner [31,51]. The boundary $\partial\Omega$ excludes regions with periodic conditions, where information from the corresponding periodic nodes is employed [12,4]. Finally, a convective velocity (\mathbf{v}_f in Eq. (7)) is interpolated at cell faces to avoid pressure-velocity decoupling on collocated meshes [40,7,12]. This convective velocity is used for the computation of the volume flux ($\mathbf{v}_f \cdot \mathbf{A}_f$) in Eq. (7). For further technical details about the finite-volume methods and computational algorithms used in this work, the reader is referred to Balcazar-Arciniega et al. [12].

3 Numerical Experiments

Systematic validations, verifications, and extensions of the Unstructured Conservative Level-Set (UCLS) method have been extensively documented in our prior works. These include studies on gravity-driven rising bubbles [7,4,3], falling droplets [6], gravity-driven bubbly flows [9,3,12,13,14], binary droplet collision [9], collision of a droplet against an interface [9], deformation of droplets under shear stresses [8], mass transfer in bubbly flows [14,2,12,13,11], and liquid-vapour phase change [5,16]. Consequently, this research represents a further step in assessing unstructured flux-limiter convective schemes for simulating transport phenomena in two-phase flows within the UCLS method framework, as proposed by Balcazar et al. [7,12,14,9,16].

Characterization of gravity-driven bubbly flow is performed by the Eötvös number $\text{Eo} = g d_b^2 (\rho_c - \rho_d) \sigma^{-1}$, Morton number $\text{Mo} = g \mu_c^4 (\rho_c - \rho_d) \rho_c^{-2} \sigma^{-3}$, viscosity ratio $\eta_\mu = \mu_c / \mu_d$, density ratio $\eta_\rho = \rho_c / \rho_d$, bubble volume fraction $\alpha = V_{\Omega_d} / V_\Omega$, and Reynolds number $\text{Re}_i(t^*) = \rho_c U_{r,i} d_b / \mu_c$, $\text{Re}(t^*) = N_b^{-1} \sum_{i=1}^{N_b} \text{Re}_i(t^*)$, $\text{Re}_i = T^{-1} \int_{t_0}^{t_0+T} \text{Re}_i(t) dt$, $\text{Re} = N_b^{-1} \sum_{i=1}^{N_b} \text{Re}_i$. Here d_b refers to the spherical equivalent bubble diameter, $V_{\Omega_{d,a}}$ is the volume of bubbles, $U_{r,i}$ is the relative velocity of the bubble respect to the velocity of Ω_c , subindex i refers to the i th bubble, and $t^* = t g^{1/2} d_b^{-1/2}$. Additionally, for the characterization of mass transfer, the following dimensionless numbers are considered: Schmidt number ($\text{Sc} = \mu_c / (\rho_c \mathcal{D}_c)$), and Sherwood number ($\text{Sh} = k_c d_b / \mathcal{D}_c$), where k_c is the mass transfer coefficient at Ω_c [12].

Figure 2 illustrates the computational setup for simulating single bubbles within an axial-symmetric domain. The domain, denoted as Ω , is discretized using 277 440

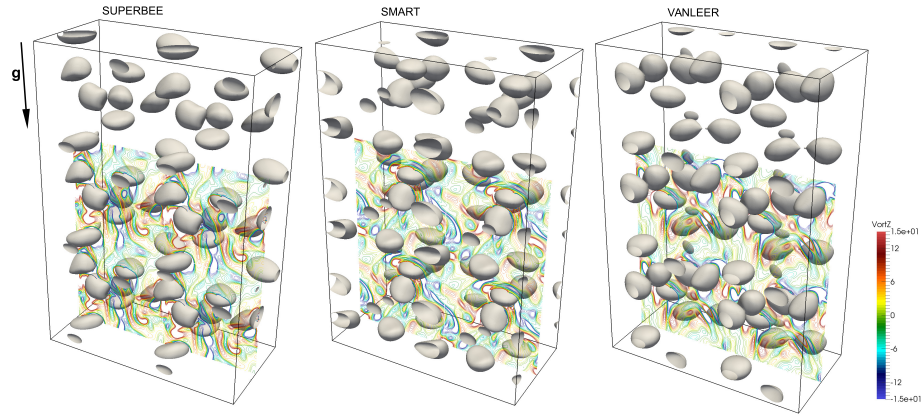


Fig. 5. Gravity-driven bubble swarm. Effect of flux-limiter convective schemes on the vorticity $\omega_z = \mathbf{e}_z \cdot (\nabla \times \mathbf{v})$. $Eo = 3$, $Mo = 10^{-8}$, $\alpha = 0.0654$, $\eta_\rho = \eta_\mu = 100$. Fully periodic domain (6 periodic cubes), $L_x = 4 d_b$, $L_y = 4 d_b$, $L_z = 4 d_b$. 150^3 uniform hexahedral control volumes, equivalent to the grid size $h = d_b/37.5$. 192 CPU-cores.

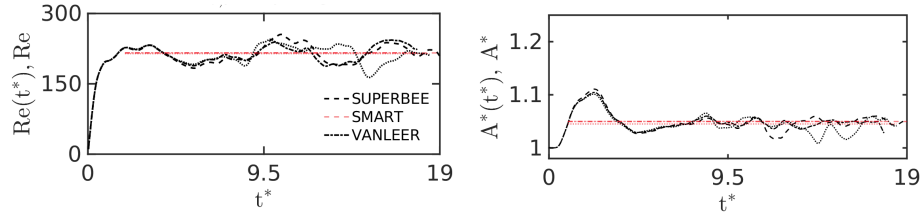


Fig. 6. Gravity-driven bubble swarm. Effect of flux-limiter convective schemes on $\{Re(t^*), A^*(t^*)\}$. $Eo = 3.0$, $Mo = 10^{-8}$, $\alpha = 0.0654$, $\eta_\rho = \eta_\mu = 100$.

hexahedral and triangular prism control volumes, with a grid resolution equivalent to solving the bubbles with $h_{\min} = d_b/40$ around the symmetry axis of Ω . This resolution has been previously validated to effectively capture the hydrodynamics and mass transfer ($Sc = 1$) within bubbles, as demonstrated in [12]. Neumann boundary conditions are applied to $\{\phi, C\}$. Concerning the velocity field \mathbf{v} , non-slip boundary conditions are applied to the top and bottom boundaries, while Neumann conditions are imposed on the lateral walls. The initial position of the bubble is set on the symmetry axis, at a distance of $2 d_b$ from the bottom boundary, with the surrounding fluids initially at rest. These simulations were performed using 14 CPUs.

The influence of flux limiters is visualized in Figure 3 and Figure 4. It is noteworthy that the SUPERBEE, KOREN, and SMART limiters effectively minimize the so-called numerical diffusion, with SUPERBEE exhibiting the least diffusion as expected. In contrast, MINMOD and UPWIND schemes introduce more numerical diffusion, with UP-

WIND being the most diffusive. The impact of these limiters is evident in the computation of $Sh(t^*)$, where the UPWIND scheme leads to a higher prediction of the Sherwood number due to this numerical artifact. Similarly, regarding the prediction of $Re(t^*)$, it is observed that the UPWIND scheme underestimates the Reynolds number compared to other limiters. The computation of the normalized area $A^* = A(t)/(\pi d_b^2)^{-1}$ is also significantly influenced by the choice of flux limiter, although SUPERBEE, SMART and KOREN limiters present closely aligned predictions.

Now, we investigate the impact of unstructured flux limiters on gravity-driven bubble swarms within a fully periodic cube denoted as Ω . The domain is discretized using 150^3 uniform hexahedral control volumes, resulting in a grid size of $h = d/40.7$. Figure 5 presents instantaneous snapshots of the z-component of the vorticity (ω_z) for SUPERBEE, SMART, and VANLEER flux limiter functions. Dimensionless parameters are set to $Eu = 3$, $Mo = 10^{-8}$, $\alpha = 0.0654$, $\eta_\rho = 100$, and $\eta_\mu = 100$. In the initial conditions, 8 bubbles are randomly distributed in the cubic domain, while the fluids remain at rest.

Figure 6 illustrates $\{Re(t^*), A^*(t^*)\}$ (black lines) and their time-averaged values $\{\overline{Re}, \overline{A^*}\}$ for the bubble swarm (depicted by red lines). It is noteworthy that the predicted $\{\overline{Re}, \overline{A^*}\}$ values exhibit remarkable consistency across SUPERBEE, SMART and VANLEER flux limiters, emphasizing their reliability and effectiveness in capturing the hydrodynamics and interfacial area of the bubble swarm.

4 Conclusions

The application of unstructured flux limiters [7,12] has proven effective in predicting hydrodynamics and mass transfer within two-phase flows. In the context of single bubble simulations, these flux limiters were specifically applied to the convective term of the transport equations, encompassing momentum, interface advection, and concentration of chemical species, as detailed in Table 1. While all evaluated flux limiters successfully prevent numerical oscillations within the framework of the UCLS method, the numerical predictions of Reynolds number and Sherwood number underscore the superior performance of the SUPERBEE limiter in minimizing numerical diffusion. Conversely, the UPWIND limiter exhibits the maximum numerical diffusion.

In relation to the hydrodynamics of bubble swarms, we observed consistent predictions for Re and Sh across the SUPERBEE, SMART, and VANLEER limiters. These results recommend their application for DNS of bubbly flows within the UCLS method framework. Our future efforts will focus on applying flux limiter schemes to intricate interface phenomena, such as the transport of surfactants on fluid interfaces and liquid-vapor phase change. These forthcoming studies aim to deepen our understanding and broaden the applicability of flux limiters in capturing complex physical interactions within multiphase systems.

References

1. Aboulhasanzadeh, B., Thomas, S., Taeibi-Rahni, M., Tryggvason, G.: Multiscale computations of mass transfer from buoyant bubbles. *Chemical Engineering Science* **75**, 456–467 (jun 2012). <https://doi.org/10.1016/j.ces.2012.04.005>, <https://linkinghub.elsevier.com/retrieve/pii/S000925091200231X>

2. Balcazar, N., Antepara, O., Rigola, J., Oliva, A.: DNS of Drag-Force and Reactive Mass Transfer in Gravity-Driven Bubbly Flows. In: García-Villalba, M., Kuerten, H., Salvetti, M. (eds) *Direct and Large Eddy Simulation XII. DLES 2019. ERCOFTAC Series*, vol 27. Springer, Cham pp. 119–125 (2020). https://doi.org/10.1007/978-3-030-42822-8_16, http://link.springer.com/10.1007/978-3-030-42822-8_16
3. Balcazar, N., Castro, J., Rigola, J., Oliva, A.: DNS of the wall effect on the motion of bubble swarms. *Procedia Computer Science* **108**, 2008–2017 (2017). <https://doi.org/10.1016/j.procs.2017.05.076>, <https://linkinghub.elsevier.com/retrieve/pii/S1877050917306142>
4. Balcazar, N., Lehmkuhl, O., Jofre, L., Oliva, A.: Level-set simulations of buoyancy-driven motion of single and multiple bubbles. *International Journal of Heat and Fluid Flow* **56** (2015). <https://doi.org/10.1016/j.ijheatfluidflow.2015.07.004>
5. Balcazar, N., Rigola, J., Oliva, A.: Unstructured Level-Set Method For Saturated Liquid-Vapor Phase Change. In: *WCCM-ECCOMAS 2020. Volume 600 - Fluid Dynamics and Transport Phenomena*. pp. 1–12 (2021). <https://doi.org/10.23967/wccm-eccomas.2020.352>, https://www.scipedia.com/public/Balcazar_et_al_2021a
6. Balcazar, N., Castro, J., Chiva, J., Oliva, A.: DNS of falling droplets in a vertical channel. *International Journal of Computational Methods and Experimental Measurements* **6**(2), 398–410 (nov 2017). <https://doi.org/10.2495/CMEM-V6-N2-398-410>, <http://www.witpress.com/doi/journals/CMEM-V6-N2-398-410>
7. Balcázar, N., Jofre, L., Lehmkuhl, O., Castro, J., Rigola, J.: A finite-volume/level-set method for simulating two-phase flows on unstructured grids. *International Journal of Multiphase Flow* **64**, 55–72 (sep 2014). <https://doi.org/10.1016/j.ijmultiphaseflow.2014.04.008>, <https://linkinghub.elsevier.com/retrieve/pii/S030193221400072X>
8. Balcazar, N., Lehmkuhl, O., Jofre, L., Rigola, J., Oliva, A.: A coupled volume-of-fluid/level-set method for simulation of two-phase flows on unstructured meshes. *Computers and Fluids* **124**, 12–29 (2016). <https://doi.org/10.1016/j.compfluid.2015.10.005>, <https://linkinghub.elsevier.com/retrieve/pii/S0045793015003394>
9. Balcazar, N., Lehmkuhl, O., Rigola, J., Oliva, A.: A multiple marker level-set method for simulation of deformable fluid particles. *International Journal of Multiphase Flow* **74**, 125–142 (2015). <https://doi.org/10.1016/j.ijmultiphaseflow.2015.04.009>
10. Balcázar, N., Rigola, J., Castro, J., Oliva, A.: A level-set model for thermocapillary motion of deformable fluid particles. *International Journal of Heat and Fluid Flow* **62**, 324–343 (dec 2016). <https://doi.org/10.1016/j.ijheatfluidflow.2016.09.015>, <https://linkinghub.elsevier.com/retrieve/pii/S0142727X16301266>
11. Balcazar-Arciniega, N., Rigola, J., Oliva, A.: DNS of Mass Transfer in Bi-dispersed Bubbly Flows in a Vertical Pipe. In: *ERCOFTAC Series*, vol. 31, pp. 55–61 (2024). https://doi.org/10.1007/978-3-031-47028-8_9, https://link.springer.com/10.1007/978-3-031-47028-8_9
12. Balcazar-Arciniega, N., Antepara, O., Rigola, J., Oliva, A.: A level-set model for mass transfer in bubbly flows. *International Journal of Heat and Mass Transfer* **138**, 335–356 (2019). <https://doi.org/10.1016/j.ijheatmasstransfer.2019.04.008>
13. Balcazar-Arciniega, N., Rigola, J., Oliva, A.: DNS of Mass Transfer from Bubbles Rising in a Vertical Channel. *Lecture Notes in Computer Science (including subseries Lecture Notes in Artificial Intelligence and Lecture Notes in Bioinformatics)* **11539 LNCS**, 596–610 (2019). https://doi.org/10.1007/978-3-030-22747-0_45, http://link.springer.com/10.1007/978-3-030-22747-0_45
14. Balcazar-Arciniega, N., Rigola, J., Oliva, A.: DNS of mass transfer in bi-dispersed bubble swarms. In: *Computational Science – ICCS 2022. ICCS 2022. Lecture*

- Notes in Computer Science, vol 13353. Springer, Cham **13353**, 284–296 (2022). https://doi.org/10.1007/978-3-031-08760-8_24, https://link.springer.com/10.1007/978-3-031-08760-8_24
15. Balcázar-Arciniega, N., Rigola, J., Oliva, A.: DNS of Thermocapillary Migration of a Bi-dispersed Suspension of Droplets. In: Computational Science – ICCS 2023. ICCS 2023. Lecture Notes in Computer Science (2016153612), 303–317 (2023). https://doi.org/10.1007/978-3-031-36030-5_25
 16. Balcázar-Arciniega, N., Rigola, J., Oliva, A.: Unstructured Conservative Level-Set (UCLS) Simulations of Film Boiling Heat Transfer. In: Computational Science – ICCS 2023. ICCS 2023. Lecture Notes in Computer Science **10477**, 318–331 (2023). <https://doi.org/10.1007/978-3-031-36030-5>, <https://link.springer.com/10.1007/978-3-031-36030-5>
 17. Bothe, D., Fleckenstein, S.: A Volume-of-Fluid-based method for mass transfer processes at fluid particles. *Chemical Engineering Science* (2013). <https://doi.org/10.1016/j.ces.2013.05.029>
 18. Brackbill, J.U., Kothe, D.B., Zemach, C.: A continuum method for modeling surface tension. *Journal of Computational Physics* **100**(2), 335–354 (1992). [https://doi.org/10.1016/0021-9991\(92\)90240-Y](https://doi.org/10.1016/0021-9991(92)90240-Y), <https://linkinghub.elsevier.com/retrieve/pii/S002199919290240Y>
 19. Chorin, A.J.: Numerical Solution of the Navier-Stokes Equations. *Mathematics of Computation* **22**(104), 745 (1968). <https://doi.org/10.2307/2004575>, <https://www.jstor.org/stable/2004575?origin=crossref>
 20. Clift, R., Grace, J., Weber, M.: *Bubbles, Drops, and Particles*. DOVER PUBLICATIONS, INC, New York (1978)
 21. Darmana, D., Deen, N.G., Kuipers, J.A.M.: Detailed 3D Modeling of Mass Transfer Processes in Two-Phase Flows with Dynamic Interfaces. *Chemical Engineering Technology* **29**(9), 1027–1033 (sep 2006). <https://doi.org/10.1002/ceat.200600156>, <https://onlinelibrary.wiley.com/doi/10.1002/ceat.200600156>
 22. Darwish, M.S., Moukalled, F.: TVD schemes for unstructured grids. *International Journal of Heat and Mass Transfer* (2003). [https://doi.org/10.1016/S0017-9310\(02\)00330-7](https://doi.org/10.1016/S0017-9310(02)00330-7)
 23. Davidson, M.R., Rudman, M.: VOLUME-OF-FLUID CALCULATION OF HEAT OR MASS TRANSFER ACROSS DEFORMING INTERFACES IN TWO-FLUID FLOW. *Numerical Heat Transfer, Part B: Fundamentals* **41**(3-4), 291–308 (mar 2002). <https://doi.org/10.1080/104077902753541023>, <http://www.tandfonline.com/doi/abs/10.1080/104077902753541023>
 24. Deen, W.: *Analysis of Transport Phenomena*. OXFORD UNIV PR (2011)
 25. Denner, F., van Wachem, B.G.: TVD differencing on three-dimensional unstructured meshes with monotonicity-preserving correction of mesh skewness. *Journal of Computational Physics* **298**, 466–479 (2015). <https://doi.org/10.1016/j.jcp.2015.06.008>
 26. Gaskell, P.H., Lau, A.K.C.: Curvature-compensated convective transport: SMART, A new boundedness-preserving transport algorithm. *International Journal for Numerical Methods in Fluids* **8**(6), 617–641 (1988). <https://doi.org/10.1002/flid.1650080602>, <http://doi.wiley.com/10.1002/flid.1650080602>
 27. Gibou, F., Fedkiw, R., Osher, S.: A review of level-set methods and some recent applications. *Journal of Computational Physics* **353**, 82–109 (jan 2018). <https://doi.org/10.1016/j.jcp.2017.10.006>, <https://linkinghub.elsevier.com/retrieve/pii/S0021999117307441>
 28. Guenther, C., Syamlal, M.: The effect of numerical diffusion on simulation of isolated bubbles in a gas-solid fluidized bed. *Powder Technology* (2001). [https://doi.org/10.1016/S0032-5910\(00\)00386-7](https://doi.org/10.1016/S0032-5910(00)00386-7)

29. Hirt, C., Nichols, B.: Volume of fluid (VOF) method for the dynamics of free boundaries. *Journal of Computational Physics* **39**(1), 201–225 (jan 1981). [https://doi.org/10.1016/0021-9991\(81\)90145-5](https://doi.org/10.1016/0021-9991(81)90145-5), <https://linkinghub.elsevier.com/retrieve/pii/S0021999181901455>
30. Hou, J., Simons, F., Hinkelmann, R.: Improved total variation diminishing schemes for advection simulation on arbitrary grids. *International Journal for Numerical Methods in Fluids* **70**(3), 359–382 (sep 2012). <https://doi.org/10.1002/flid.2700>
31. Karniadakis, G.E., Kirby II, R.M.: *Parallel Scientific Computing in C++ and MPI*. Cambridge University Press (jun 2003). <https://doi.org/10.1017/CBO9780511812583>, <https://www.cambridge.org/core/product/identifier/9780511812583/type/book>
32. Koren, B.: A Robust Upwind Discretization Method for Advection, Diffusion and Source Terms. In: *Numerical Methods for Advection-Diffusion Problems*, C. Vreugdenhil and B. Koren, eds., vol. 45 of *Notes on Numerical Fluid Mechanics*, Vieweg, Braunschweig pp. 117–138 (1993)
33. Koynov, A., Khinast, J.G., Tryggvason, G.: Mass transfer and chemical reactions in bubble swarms with dynamic interfaces. *AIChE Journal* **51**(10), 2786–2800 (oct 2005). <https://doi.org/10.1002/aic.10529>, <https://onlinelibrary.wiley.com/doi/10.1002/aic.10529>
34. LeVeque, R.J.: High-Resolution Conservative Algorithms for Advection in Incompressible Flow. *SIAM Journal on Numerical Analysis* **33**(2), 627–665 (apr 1996). <https://doi.org/10.1137/0733033>
35. LeVeque, R.J.: *Finite Volume Methods for Hyperbolic Problems* (2002). <https://doi.org/10.1017/cbo9780511791253>
36. Olsson, E., Kreiss, G.: A conservative level set method for two phase flow. *Journal of Computational Physics* **210**(1), 225–246 (nov 2005). <https://doi.org/10.1016/j.jcp.2005.04.007>, <https://linkinghub.elsevier.com/retrieve/pii/S0021999105002184>
37. Osher, S., Sethian, J.A.: Fronts propagating with curvature-dependent speed: Algorithms based on Hamilton-Jacobi formulations. *Journal of Computational Physics* **79**(1), 12–49 (nov 1988). [https://doi.org/10.1016/0021-9991\(88\)90002-2](https://doi.org/10.1016/0021-9991(88)90002-2), <https://linkinghub.elsevier.com/retrieve/pii/0021999188900022>
38. Patankar, S.V.: *Numerical Heat Transfer and Fluid Flow*. Taylor & Francis (1980)
39. Prosperetti, A., Tryggvason, G.: *Computational Methods for Multiphase Flow*. Cambridge University Press, Cambridge (2007). <https://doi.org/10.1017/CBO9780511607486>
40. Rhie, C.M., Chow, W.L.: Numerical study of the turbulent flow past an airfoil with trailing edge separation. *AIAA Journal* **21**(11), 1525–1532 (1983). <https://doi.org/10.2514/3.8284>, <https://arc.aiaa.org/doi/10.2514/3.8284>
41. Roghair, I., Van Sint Annaland, M., Kuipers, J.: An improved Front-Tracking technique for the simulation of mass transfer in dense bubbly flows. *Chemical Engineering Science* **152**, 351–369 (oct 2016). <https://doi.org/10.1016/j.ces.2016.06.026>, <https://linkinghub.elsevier.com/retrieve/pii/S0009250916303268>
42. Sun, D., Tao, W.: A coupled volume-of-fluid and level set (VOSET) method for computing incompressible two-phase flows. *International Journal of Heat and Mass Transfer* **53**(4), 645–655 (jan 2010). <https://doi.org/10.1016/j.ijheatmasstransfer.2009.10.030>, <https://linkinghub.elsevier.com/retrieve/pii/S0017931009005717>
43. Sussman, M., Puckett, E.G.: A Coupled Level Set and Volume-of-Fluid Method for Computing 3D and Axisymmetric Incompressible Two-Phase Flows. *Journal of Computational Physics* **162**(2), 301–337 (aug 2000). <https://doi.org/10.1006/jcph.2000.6537>, <https://linkinghub.elsevier.com/retrieve/pii/S0021999100965379>

44. Sussman, M., Smereka, P., Osher, S.: A Level Set Approach for Computing Solutions to Incompressible Two-Phase Flow. *Journal of Computational Physics* **114**(1), 146–159 (sep 1994). <https://doi.org/10.1006/jcph.1994.1155>, <https://linkinghub.elsevier.com/retrieve/pii/S0021999184711557>
45. Sussman, M., Smereka, P., Osher, S.: A Level Set Approach for Computing Solutions to Incompressible Two-Phase Flow. *Journal of Computational Physics* **114**(1), 146–159 (sep 1994). <https://doi.org/10.1006/jcph.1994.1155>, <https://linkinghub.elsevier.com/retrieve/pii/S0021999184711557>
46. Sweby, P.K.: HIGH RESOLUTION SCHEMES USING FLUX LIMITERS FOR HYPERBOLIC CONSERVATION LAWS. *SIAM Journal on Numerical Analysis* (1984). <https://doi.org/10.1137/0721062>
47. Sweby, P.K.: High Resolution Schemes Using Flux Limiters for Hyperbolic Conservation Laws. *SIAM Journal on Numerical Analysis* **21**(5), 995–1011 (oct 1984). <https://doi.org/10.1137/0721062>, <http://epubs.siam.org/doi/10.1137/0721062>
48. Tryggvason, G., Bunner, B., Esmaceli, A., Juric, D., Al-Rawahi, N., Tauber, W., Han, J., Nas, S., Jan, Y.J.: A Front-Tracking Method for the Computations of Multiphase Flow. *Journal of Computational Physics* **169**(2), 708–759 (may 2001). <https://doi.org/10.1006/jcph.2001.6726>, <https://linkinghub.elsevier.com/retrieve/pii/S0021999101967269>
49. Tryggvason, G., Scardovelli, R., Zaleski, S.: Direct Numerical Simulations of Gas–Liquid Multiphase Flows (2001). <https://doi.org/10.1017/CBO9780511975264>, <https://www.cambridge.org/core/product/identifier/9780511975264/type/book>
50. Unverdi, S.O., Tryggvason, G.: A front-tracking method for viscous, incompressible, multi-fluid flows. *Journal of Computational Physics* **100**(1), 25–37 (may 1992). [https://doi.org/10.1016/0021-9991\(92\)90307-K](https://doi.org/10.1016/0021-9991(92)90307-K), <https://linkinghub.elsevier.com/retrieve/pii/002199919290307K>
51. Van der Vorst, H.A., Dekker, K.: Conjugate gradient type methods and preconditioning. *Journal of Computational and Applied Mathematics* **24**(1-2), 73–87 (nov 1988). [https://doi.org/10.1016/0377-0427\(88\)90344-5](https://doi.org/10.1016/0377-0427(88)90344-5), <https://linkinghub.elsevier.com/retrieve/pii/0377042788903445>
52. Zhang, D., Jiang, C., Cheng, L., Liang, D.: A refined r-factor algorithm for TVD schemes on arbitrary unstructured meshes. *International Journal for Numerical Methods in Fluids* **80**(2), 105–139 (jan 2016). <https://doi.org/10.1002/flid.4073>